First-principles study of phonon linewidths in noble metals

Xiaoli Tang and B. Fultz

Phys. Rev. B **84**, 054303 — Published 9 August 2011

DOI: 10.1103/PhysRevB.84.054303

A first-principles study of phonon linewidths in noble metals

Xiaoli Tang and B. Fultz[1]

[1] *Department of Applied Physics and Materials Science, California Institute of Technology, Pasadena, California 91125, USA*

Phonon lifetimes in Cu, Ag and Au at low and high temperatures were calculated along high symmetry directions using density functional theory combined with second-order perturbation theory. Both harmonic and third-order anharmonic force constants were computed using a supercell small displacement method, and the two-phonon densities of states were calculated for all three-phonon processes consistent with the kinematics of energy and momentum conservation. A non-rigorous Grüneisen model with no q-dependence of the anharmonic coupling constants offers a simple separation of the potential and the kinematics, and proved semi-quantitative for Cu, Ag and Au. A rule is reported for finding the most anharmonic phonon mode in fcc metals.

I. INTRODUCTION

At elevated temperatures, phonon thermodynamics exhibits phenomena beyond the harmonic model of lattice vibrations. Heat capacities inconsistent with the Dulong-Petit limit, thermal expansion, and finite thermal conductivity are well known non-harmonic effects. Sometimes the harmonic model can be adapted through the "quasiharmonic model" to explain these effects. A quasiharmonic model assumes harmonic phonons with infinite lifetimes, but with frequencies lowered (softened) owing to thermal expansion. To account for finite phonon lifetimes, other effects such as phonon-phonon interactions or electron-phonon interactions must be considered.

In our previous study of aluminum[1], a simple fcc nearly free electron metal, we found that phonon-phonon interactions dominate the phonon energy linewidth at elevated temperatures. The phonon linewidth distribution over the whole Brillouin zone shows clear locations of the most anharmonic phonon modes. This trend is mirrored in the two-phonon density of states that characterizes the total density of available states for the decay or excitation of phonons in three-phonon processes. Since the two-phonon density of states is determined by the phonon dispersions, a systematic study of similar fcc metals with different phonon dispersions is helpful for identifying the interesting physics. We selected three noble metals, Cu, Ag and Au, that have very low densities of states near the Fermi level so electron-phonon interactions are small[2].

Phonon-phonon interactions are responsible for the phonon scattering processes that underly thermal resistivity, a topic of current interest for thermoelectric materials and thermal barrier coatings, for example. Phonon lifetimes are a measure of these scattering processes, but there have been few systematic studies of phonon lifetimes besides optical measurements. For noble metals, work on phonon damping includes only one experimental study on copper[3] and one theoretical calculation using an empirical method that relates the anharmonic force constants to experimental third-order elastic moduli[4]. The mathematical form of the interatomic potential in the latter study contains numerous fitting parameters, and its final form is somewhat uncertain. Furthermore, anharmonic elastic moduli are not always available experimentally. A parameter-free first-principles approach is therefore valuable for exploring the microscopic physics of phonon-phonon scattering.

There are two general approaches for calculating phonon linewidth or lifetime from first principles. The first is based on anharmonic perturbation theory[5,6], where the anharmonic energy is treated as a perturbation to the harmonic energy. The coupling constants between the harmonic phonons are obtained through lattice dynamics calculations. The other approach is to analyze the normal mode correlation functions obtained by molecular dynamics (MD) simulations (e.g.[7]). The MD approach has the advantage that it includes all the anharmonicity, but it is usually restricted to high temperatures where the atomic motion is treated classically. In the perturbation theory approach, the main challenge is to calculate the phonon coupling constants. Usually only the dominant third-order anharmonicity and three-phonon scattering processes are considered for phonon linewidths, but this has proved successful[1]. The anharmonic force constants can be obtained either by the direct supercell method or by the reciprocal response method. The latter applies the "2n+1"theorem to determine the cubic coupling coefficients in the framework of density-functional perturbation theory[8,9]. Although only unit cell is necessary in the response method, it must be hard-coded at the level of the wave-function. On the other hand, calculating directly the anharmonic force constants with a supercell technique can be done with any computational package that calculates forces from either ab-initio or empirical potentials.

Here we report results from a systematic study on phonon energy broadening from phonon-phonon interactions in the noble metals Cu, Ag, and Au using the direct supercell method combined with density functional theory (DFT) for lattice dynamics calculations. We first overview the theory and computational methodology, then show calculated phonon linewidths of the three metals and their temperature dependence. We also present the leading anharmonic force constants, the kinematic scattering mechanisms, and compare these three metal systems. Finally, the results of a simplified model of phonon linewidths are discussed.

II. COMPUTATIONAL METHODOLOGY

The essential inputs for phonon linewidth calculations with the direct supercell method are the harmonic and third-order anharmonic force constants that appear in the Taylor expansion of the total energy E with respect to atomic displacements u:

$$E = E_0 + \sum_i F_i u_i + \frac{1}{2!}\sum_{ij}\phi_{ij}u_i u_j + \frac{1}{3!}\sum_{ijm}\phi_{ijm}u_i u_j u_m + \frac{1}{4!}\sum_{ijmn}\phi_{ijmn}u_i u_j u_m u_n + \dots \quad (1)$$

Here E_0 is the total energy of the crystal when all the atoms are fixed at their equilibrium positions. The second term is zero when the system is in equilibrium. The third term is the harmonic contribution to the total energy and the fourth terms and beyond are the anharmonic contributions to the total energy. The coefficients in the expansion (from left to right) are forces F_i, harmonic force constants ϕ_{ij}, and cubic and quartic anharmonic force constants ϕ_{ijm} and ϕ_{ijmn}. The index i denotes a set (l, k, α), where l is the unit cell index, k is the atom index in the unit cell, and α is the index for cartesian coordinates.

Within the harmonic approximation, which considers up to the quadratic terms in the total energy expansion of Eqn. 1, phonons are independent, non-interacting quasi-particles with infinite lifetimes. To account for finite lifetimes, higher-order terms are needed. To the lowest order of perturbation, the cubic term dominates. Considering the cubic anharmonic energy as a perturbation to the harmonic system, the inverse of phonon lifetime, 2Γ, derived from second order perturbation theory[5,6] within the single-mode relaxation approximation is:

$$\begin{aligned} 2\Gamma(\mathbf{q}, j) = \frac{\pi\hbar}{8N} \sum_{\mathbf{q}_1, \mathbf{q}_2, j_1, j_2} \Delta(\mathbf{q}_1 + \mathbf{q}_2 - \mathbf{q}) \frac{|\Phi(-\mathbf{q}j;\, \mathbf{q}_1 j_1;\, \mathbf{q}_2 j_2)|^2}{\omega(\mathbf{q}j)\, \omega(\mathbf{q}_1 j_1)\, \omega(\mathbf{q}_2 j_2)} \\ \times \left[(n_1 + n_2 + 1)\, \delta(\omega - \omega_1 - \omega_2) \right. \\ \left. + 2(n_1 - n_2)\, \delta(\omega + \omega_1 - \omega_2) \right] , \end{aligned} \tag{2}$$

where N is the number of unit cells, $\hbar$ is the Planck constant, and n is the Planck distribution function. Φ is the Fourier transform of the third-order lattice anharmonic tensor:

$$\begin{aligned} \Phi(-\mathbf{q}j; \mathbf{q}_1 j_1; \mathbf{q}_2 j_2) = & \sum_{kk'k'', \alpha\beta\gamma} e_\alpha(k|-\mathbf{q}j) e_\beta(k'|\mathbf{q}_1 j_1) e_\gamma(k''|\mathbf{q}_2 j_2) \\ & \times \frac{1}{\sqrt{m_k m_{k'} m_{k''}}} \sum_{ll'} [\phi_{\alpha\beta\gamma}(0k, lk', l'k'') \\ & \times \mathrm{e}^{\mathrm{i}(-\mathbf{q}\cdot\mathbf{R}(0k) + \mathbf{q}_1 \cdot \mathbf{R}(lk') + \mathbf{q}_2 \cdot \mathbf{R}(l'k''))}] , \end{aligned} \tag{3}$$

and $\omega(\mathbf{q}, j)$ is the phonon energy with wavevector $\mathbf{q}$ and branch index j, obtained by diagonalizing the dynamical matrix $\mathbf{D}$:

$$\omega^2(\mathbf{q}, j)\mathbf{e}(\mathbf{q}, j) = \mathbf{D}(\mathbf{q})\mathbf{e}(\mathbf{q}, j) , \tag{4}$$

where

$$\mathbf{D}(\mathbf{q}) = \frac{1}{m_k m_{k'}} \sum_l \phi_{\alpha\beta}(0k, lk') \mathrm{e}^{\mathrm{i}\mathbf{q}\cdot(\mathbf{R}(l'k') - \mathbf{R}(lk))} , \tag{5}$$

and $\mathbf{e}(\mathbf{q}, i)$ is the eigenvector of mode $(\mathbf{q}, i)$, and m_k is the mass the k^{th} atom in the unit cell. $\mathbf{R}(l, k)$ is the position of the k^{th} atom in the l^{th} unit cell.

With Eqns. 1-5, calculations of phonon linewidths require second-order harmonic and third-order anharmonic force constants, which can be obtained ab initio. In the supercell method, the force constants are obtained from small displacements of atoms Δ, and the Hellmann-Feynman theorem. Accurate calculations of forces, however, require the computational cells to be large enough so the interaction between the displaced atom and its image outside the supercell is negligible. In addition, the strategy of both positive and negative displacement is often used, which not only reduces numerical risks from small displacements, but also eliminates the effect from higher-order anharmonicity. This construction allows the calculation of harmonic force constants:

$$\begin{aligned} \phi_{ij} = \frac{1}{12\Delta} [& -8F_i(u_j = \Delta) + 8F_i(u_j = -\Delta) \\ & + F_i(u_j = 2\Delta) - F_i(u_j = -2\Delta)] , \end{aligned} \tag{6}$$

the semidiagonal cubic force constants:

$$\begin{aligned} \phi_{ijj} = \frac{1}{3\Delta^2} [& F_i(u_j = \Delta) + F_i(u_j = -\Delta) \\ & - F_i(u_j = 2\Delta) - F_i(u_j = -2\Delta)] , \end{aligned} \tag{7}$$

and nondiagonal cubic force constants:

$$\begin{aligned} \phi_{ijk} = \frac{1}{4\Delta^2} [& -F_i(u_j = \Delta, u_k = \Delta) + F_i(u_j = \Delta, u_k = -\Delta) \\ & + F_i(u_j = -\Delta, u_k = \Delta) - F_i(u_j = -\Delta, u_k = -\Delta)] . \end{aligned} \tag{8}$$

The practical implementation starts with determining the independent harmonic and anharmonic force constants for the supercell, followed by ab-initio calculations of atomic forces from the displacements of a single atom or a pair of atoms in the supercell. The force constants are then constructed using Eqns. 6-8. Equations 3-5 are used to compute the harmonic phonon characteristics and anharmonic phonon coupling constants, from which the phonon linewidths are evaluated using Eqn. 2. Numerical issues include the choice of small displacements and the enforcement of sum rules for the force constant matrix. The symmetry of force constant elements has been taken care of automatically in the symmetry analysis for the independent tensor elements.

The present study of phonon linewidths of noble metals used the VASP package[10–12] and Blöchl's projector augmented wave (PAW) potentials[13,14] for all energy and force calculations with DFT. Both the local density approximation (LDA) and the generalized gradient approximation (GGA) for the exchange-correlation functional were used. The functional that gave better phonon dispersions was used for the linewidth calculations. The electronic structure was calculated self-consistently using a $24 \times 24 \times 24$ k-grid for 1-atom unit cells. The choice of 0.1 eV for the Methfessel-Paxton smearing and the default plane wave energy cutoff in the pseudopotentials consistently gave converged energies for all three metals. The ground state structure found by fitting the energy-volume relationship to the third-order Birch-Murnaghan equation of state was used in the subsequent calculations. Convergence with respect to the supercell size and k-point sampling was tested thoroughly in the previous study of lattice dynamics of fcc metals by Grabowski *et al.*[15]. To calculate forces accurately, we used the same large 256-atom supercells ($4 \times 4 \times 4$ conventional fcc unit cell) and a k-point sampling grid of $3 \times 3 \times 3$. The augmentation grid was exactly twice as large as the coarse grid for representation of the pseudo wavefunctions. An additional grid was switched on to help reduce the noise in the forces. By symmetry, there are in total 55 independent harmonic force constants and 6205 independent third-order anharmonic force constants in a 256-atom fcc Bravias supercell lattice, leading to 1 or 272 irreducible distorted supercells with one atom or a pair of atoms displaced from their equilibrium positions. Both positive and negative displacements of 0.02 Å were used to cancel effects from higher-order anharmonicities. Phonon linewidths were calculated with Eqn. 2 using a $24 \times 24 \times 24$ q-point grid with an additional $32 \times 32 \times 32$ interpolation within the prism around each q-point, giving well-converged results.

Anharmonicity is affected by the longer-range parts of the potential. Although large supercells and fine k-grids were needed to obtain accurate forces, anharmonic force constants were found to decay rapidly with interatomic distance. The leading contributions to the phonon linewidths were from the nearest neighbor coupling constants. Phonon linewidths from calculations that include anharmonic constants from more distant neighbor shells were compared, but the differences were small. So the leading contribution of linewidths from the nearest neighbor anharmonic interactions are presented in this study.

III. RESULTS

Table I presents the equilibrium lattice constants predicted from ab-initio DFT calculations using the LDA and GGA density functionals with comparison to experimental results. It is known that LDA underestimate the lattice constant while GGA overestimates it. Our results are consistent with this general trend, but GGA gives lattice constants for copper in better agreement with experiment, whereas LDA does better for gold. Both GGA and LDA give lattice constants for silver of similar difference from the experimental value.

TABLE I. Lattice constants (Å) of noble metals from both LDA and GGA PAW-potentials and experimental room temperature values. Deviations from experimental lattice constants are in parenthesis.

Metal System	LDA-PAW	GGA-PAW	Experiment
Cu	3.5246(-2.36%)	3.6452(+0.97%)	3.61
Ag	4.0158(-1.81%)	4.1623(+1.77%)	4.09
Au	4.0613(-0.46%)	4.1748(+2.32%)	4.08

Figure 1 shows the calculated phonon dispersions of three noble metals at calculated equilibrium volumes at 0 K. As for the prediction of lattice constant, GGA gives Cu phonon dispersions in much better agreement with experiment than LDA, while LDA does better for Au. While excellent agreement between experiment and calculations are seen for both Cu and Au, there is a notable difference for Ag using either functional, although LDA is slightly better. This discrepancy was reported previously[15]. Further tests were made with a larger supercell (500 atoms) and finer k-grid ($4 \times 4 \times 4$), the improvement was minimal. Hence we attribute the discrepancy for Ag to the exchange-correlation functional rather than computational issues. Since the phonon dispersions serve as the basis set for the phonon linewidth calculations, the potential that gave phonon dispersions with better agreement with experiment was used

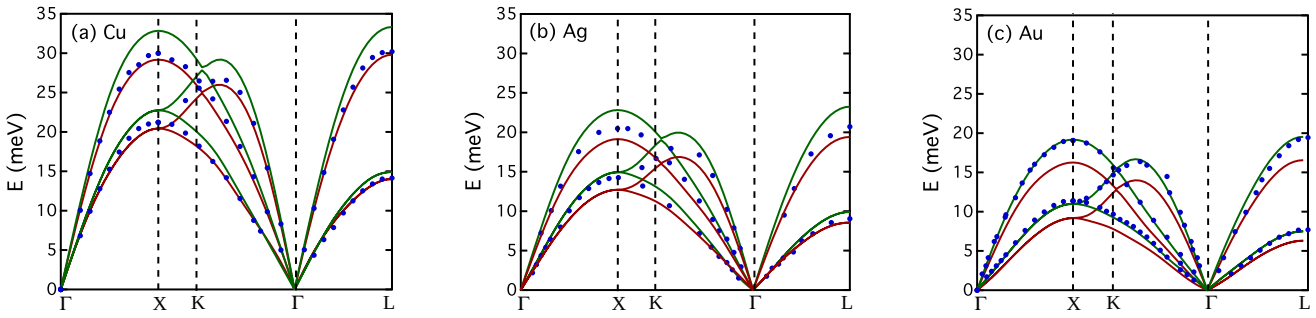

FIG. 1. Phonon dispersions of (a) copper, (b) silver, and (c) gold along high-symmetry directions calculated using both LDA (green) and GGA (red) exchange-correlation functionals. The experimental points are from Ref.[16].

for phonon linewidth calculations, *i.e.*, the GGA PAW-potential was used for Cu, and the LDA PAW-potential was used for Ag and Au.

As shown in Eqn. 2, the phonon linewidth is determined by both phonon scattering kinematics and phonon coupling constants. The kinematics originates with the phonon dispersions, *i.e.*, the energy-momentum relationships of all the phonons, whereas the coupling constants are closely related to the anharmonicity of the interatomic potentials. Table II lists the dominant third-order anharmonic force constants for different atom pairs in the first-, second- and third-neighbor shells calculated from a 256-atom supercell model. Harmonic force constants are listed for comparison. While the onsite force constants are the largest harmonic terms for these fcc metals, the corresponding third-order onsite force constants vanish by symmetry. The dominant third-order force constants are the bond-stretching forces between the reference atom and its nearest neighbor. The corresponding bond-bending force constants for nearest-neighbor pairs (not listed) are smaller by one order of magnitude. For the reference atom and its second- or higher-nearest neighbors, both bond-stretching and bond-bending anharmonic force constants are one order of magnitude smaller than those from the nearest-neighbor interactions. The differences in the anharmonic forces between second-, third- and fourth-neighbor interactions are much less. The leading anharmonic force constants increase from Cu to Ag to Au, indicating an increase of anharmonicity.

TABLE II. Leading harmonic and anharmonic bond-stretching force constants of neighboring pairs from different shells. The bond direction is rotated to be along z-axis by covariant transformation. 1 and 2 denote first and second atom, $1^{st}, 2^{nd}, 3^{rd}$ denote the neighboring shell of the second atom. Harmonic and third-order anharmonic force constants have units of eV/Å^2 and eV/Å^3 respectively.

	ϕ^{111}_{zzz}	ϕ^{11}_{zz}	ϕ^{112}_{zzz}			ϕ^{12}_{zz}		
	onsite		1^{st}	2^{nd}	3^{rd}	1^{st}	2^{nd}	3^{rd}
Cu	0	6.569	-9.312	0.061	0.028	-1.678	-0.067	-0.048
Ag	0	6.213	-9.40	-0.042	0.018	-1.802	-0.082	-0.037
Au	0	7.127	-12.50	-0.297	-0.006	-2.397	-0.267	-0.032

While the third-order phonon coupling constants affect the coupling strength between phonons in three-phonon scattering processes, a prerequisite is that these three phonons satisfy the kinematic condition of momentum and energy conservation. As defined previously[1], the kinematics can be categorized into down-conversion processes $D_\downarrow$ and up-conversion processes $D_\uparrow$:

$$D_\downarrow(i,\mathbf{q}) = \tfrac{1}{N}\sum_{\mathbf{q}_1,\mathbf{q}_2,j_1,j_2} \Delta(\mathbf{q}-\mathbf{q}_1-\mathbf{q}_2)\,\delta(\omega-\omega_1-\omega_2)\,, \tag{9}$$

$$D_\uparrow(i,\mathbf{q}) = \tfrac{1}{N}\sum_{\mathbf{q}_1,\mathbf{q}_2,j_1,j_2} \Delta(\mathbf{q}+\mathbf{q}_1-\mathbf{q}_2)\,\delta(\omega+\omega_1-\omega_2)\,. \tag{10}$$

Owing to energy and momentum conservation, down-conversion processes are kinematically forbidden for the lower-energy transverse phonons TA_1. A generalization of this rule has been proved – a phonon cannot decay by any anharmonic process into a set of phonons of higher phase velocity[17]. As we reported for aluminum[1], TA phonons are scattered mostly by up-conversion processes; LA phonons, especially short-wavelength ones, are scattered mostly by down-conversion processes (Fig. 2). Table III lists the relative contributions from different scattering processes for

TABLE III. Percentage of different scattering processes for LA and TA modes near X-point of zone boundary and near zone center Γ.

$q \to$ X							
LA	TA+TA	LA+LA	LA+TA	TA	TA-TA	LA-LA	LA-TA
Cu	98.2%	0.0%	1.8%	Cu	0.0%	7.9%	92.1%
Ag	95.8%	0.0%	4.2%	Ag	0.0%	6.1%	93.9%
Au	91.0%	0.0%	9.0%	Au	0.0%	2.2%	97.8%
$q \to \Gamma$							
LA	TA-TA	LA-LA	LA-TA	TA	TA-TA	LA-LA	LA-TA
Cu	90.4%	0.0%	9.6%	Cu	79.4%	14.0%	6.6%
Ag	91.4%	0.5%	8.1%	Ag	73.0%	24.7%	2.3%
Au	94.2%	0.2%	5.6%	Au	79.2%	20.3%	0.5%

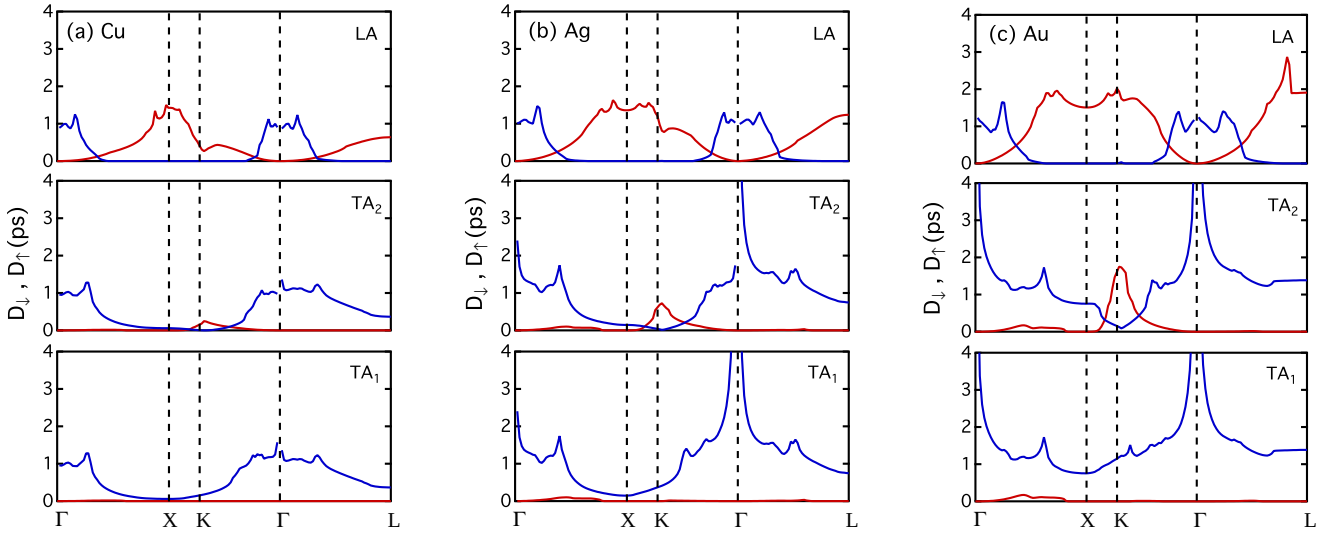

FIG. 2. Two-phonon density of states of copper (a), silver (b), and gold (c) along high-symmetry directions. $D_\downarrow$ in red shows the down-conversion processes and $D_\uparrow$ in blue shows the up-conversion processes.

both LA and TA modes near zone boundaries and the zone center. The dominant decay channels for short-wavelength LA phonons are LA↔TA+TA and LA↔LA+TA. Towards the zone center, fewer down-conversion channels become available, and up-conversion channels start to open for LA phonons at q-vectors where their energies are lower than some TA phonons. Scattering channels change from LA↔LA-TA dominance to LA↔TA-TA dominance as the q-vector approaches the zone center. From the symmetry of the scattering channels, the dominant scattering channels for TA phonons near the zone boundary are TA↔LA-TA. Near the zone center, processes like TA↔TA-TA and TA↔LA-LA start to dominate for the TA phonons.

Across Fig. 2, one sees notable differences in the $D_\downarrow$ and $D_\uparrow$ processes for Cu, Ag and Au, indicating differences in the number of scattering channels for each mode. Figure 3 shows the linewidths of phonon modes at three representative temperatures along the same high symmetry directions, where the GGA PAW-potential for Cu and the LDA PAW-potential for Ag and Au were used in the linewidth calculations. The room temperature phonon linewidths from the prior neutron scattering measurements[3] are about twice as large as our calculated linewidths. (Curiously, the temperature dependences of the measured linewidths are much smaller, and sometimes almost negligible.) Despite the large differences between Cu, Ag and Au, their phonon linewidths are comparable, and have similar trends along crystallographic directions. Nevertheless, the phonon linewidth does not change monotonically with q vector as does the phonon energy. These three metals have different locations for their most anharmonic phonons. Along the Γ-X direction, the phonon of broadest linewidth in Cu is at the X-point (1,0,0), but is at about (5/6,0,0) in Ag and (2/3,0,0) in Au. These features are also seen in Fig. 2. Comparing to previous results from an empirical model by Zoli, *et al.*[4], we find peaks in linewidth at similar locations on the LA and TA branches, and we find the phonon linewidths at room temperature are comparable. (The peak in the broadening on the LA branch of Ag was missed in

the previous study, however, since it lies between the five calculated data points.)

Figure 3 also shows the effect of temperature on phonon broadening. Since the scattering rate of a phonon is proportional to the occupation number of the other two phonons, phonon linewidths increase with temperature. At 0 K, the linewidths of the lowest energy TA modes are zero because the up-conversion contribution vanishes as $T \to 0$, whereas LA modes have small linewidths (less than 0.2 meV) because down conversion processes have a finite value due to the spontaneous decay of a phonon into two lower-energy phonons. At high temperatures, the phonon occupation number increases linearly with temperature, and so does the phonon linewidth. These noble metals all have Debye temperatures below room temperature, so linewidths calculated at 300 K and 600 K are approximately in the linear region. The proportionality can be estimated from the increase of phonon linewidth from 300 K to 600 K. For example, the LA mode of Cu at the X-point has a linewidth about 2 meV at 300 K (6.7% of its energy), and increases to 3.9 meV at 600 K (13% of its energy if neglecting thermal expansion). This gives a rate of increase of linewidth of 0.006 meV K^{-1}, or a rate of decrease of quality factor ($\frac{\omega}{2\Gamma}$) of 0.021% K^{-1}.

Three-phonon processes are categorized as normal processes or umklapp processes, depending on whether or not a reciprocal lattice vector is needed for momentum conservation. For fcc noble metals, umklapp processes contribute nearly 90% of the phonon linewidth. If we decompose the contribution to the linewidth to down-conversion and up-conversion processes, we find down-conversion processes contribute about 99% of the phonon linewidth of LA modes, while the linewidths of TA modes are mostly from the up-conversion processes.

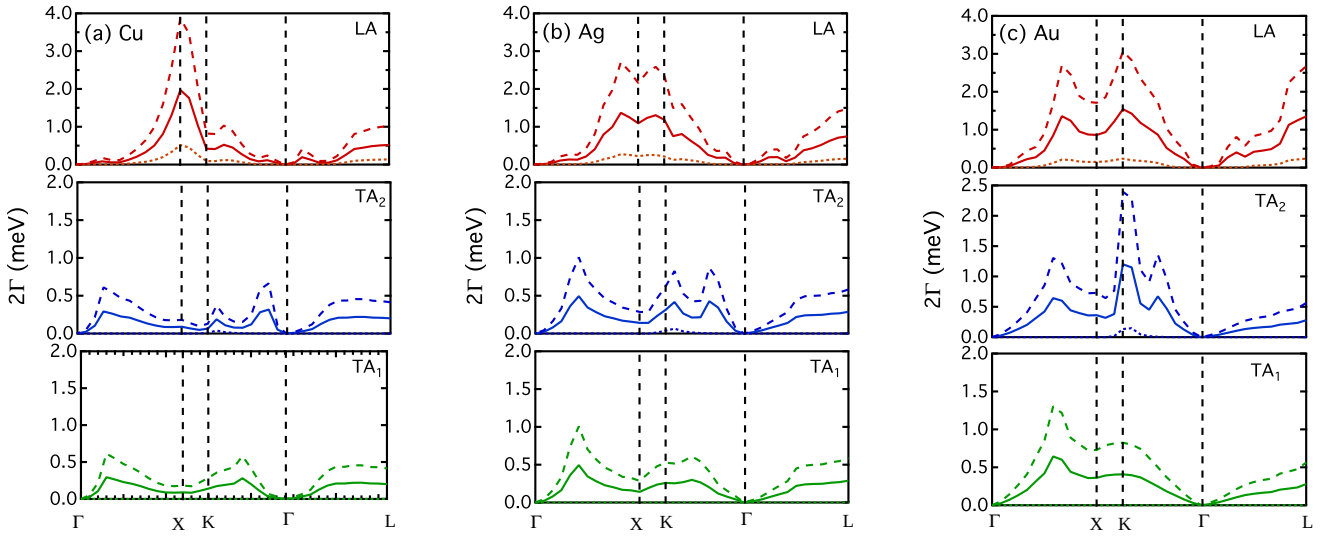

FIG. 3. Phonon linewiths of (a) copper, (b) silver, and (c) gold along high-symmetry directions at 0 K (dotted-line), 300 K (solid line) and 600 K (dashed line).

IV. DISCUSSION

Both the anharmonicity of the potential and the kinematics of phonon scattering contribute to the overall linewidth, but the decoupling of these two effects is not straightforward. On the other hand, we do see common features in the two-phonon densities of states $D_\downarrow$ and $D_\uparrow$ and the phonon linewidth 2Γ, especially in the outer parts of the Brillouin zone. This correspondence suggests an approximation of ignoring the q-dependence of Φ in Eqn. 2, and separating an anharmonic potential factor from a kinematic factor when calculating phonon linewidths. Although this is not rigorous, we explore this approximation in what follows, and we find that it has at least semi-quantitative success for fcc Cu, Ag, and Au.

A comparison of Figs. 2 and 3 shows that the broadening contribution from the dominant up-conversion processes is suppressed in the inner part of Brillouin zone near Γ. An explanation can be found in a simplified Grüneisen model for the phonon coupling constants proposed by Klemens[18]:

$$\Phi(\mathbf{q}j;\mathbf{q}_1j_1;\mathbf{q}_2j_2) = \frac{2i\gamma}{\sqrt{(3m)v}}\omega(\mathbf{q}j)\omega(\mathbf{q_1}j_1)\omega(\mathbf{q_2}j_2)\ , \tag{11}$$

where γ is the Grüneisen parameter, v is the sound velocity, and m is the mass of the atom. Using Eqn. 11 in Eqn. 2, and considering the high temperature limit so $\hbar\omega \ll k_B T$ and $n = \frac{k_B T}{\hbar\omega} \gg 1$,

$$(n_1 + n_2 + 1)\delta(\omega - \omega_1 - \omega_2) \simeq \frac{k_B T}{\hbar} \frac{\omega(\mathbf{q}j)}{\omega(\mathbf{q}_1 j_1)\omega(\mathbf{q}_2 j_2)} , \tag{12}$$

and

$$(n_1 - n_2)\delta(\omega + \omega_1 - \omega_2) \simeq \frac{k_B T}{\hbar} \frac{\omega(\mathbf{q}j)}{\omega(\mathbf{q}_1 j_1)\omega(\mathbf{q}_2 j_2)} , \tag{13}$$

so Eqn. 2 is reduced to

$$2\Gamma(\mathbf{q}, j) = \frac{\pi k_B T}{6} \frac{\gamma^2 \omega(\mathbf{q}, j)^2}{mv^2} (D_\downarrow(\mathbf{q}, j) + 2D_\uparrow(\mathbf{q}, j)) . \tag{14}$$

In the low temperature limit as $T \to 0$, the phonon occupation number $n \to 0$, and only down-conversion processes $D_\downarrow$ contribute to the phonon broadening. Since the final state energy spectra are symmetric with half of the energy of the decay phonon, Okubo and Tamura[20] made a further approximation that $\omega(\mathbf{q}_1 j_1) = \omega(\mathbf{q}_2 j_2) = \frac{\omega(\mathbf{q}j)}{2}$, reducing Eqn. 2 to

$$2\Gamma(\mathbf{q}, j) = \frac{\pi\hbar}{24} \frac{\gamma^2 \omega(\mathbf{q}, j)^3}{mv^2} D_\downarrow(\mathbf{q}, j) . \tag{15}$$

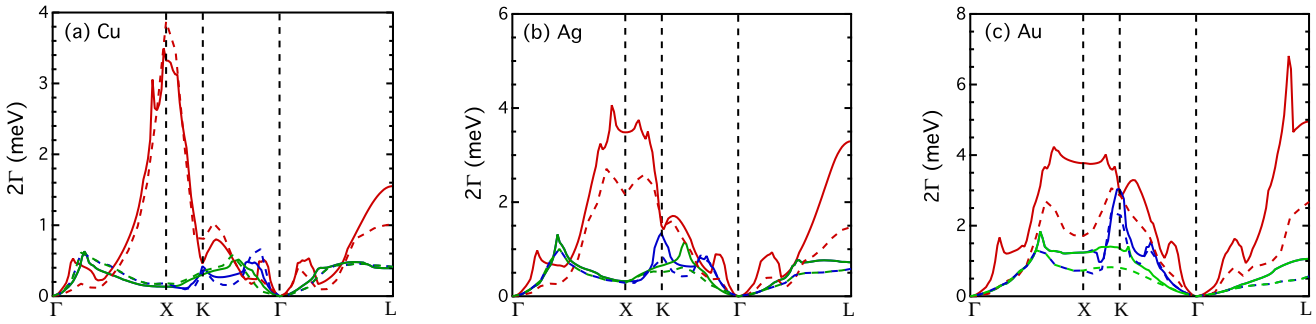

FIG. 4. Comparison of phonon linewidth for (a) copper, (b) silver, and (c) gold along high-symmetry directions at 600 K between model predictions (solid-line) based on Eqn. 14 and direct calculations (dashed-line) from Fig. 3. LA branch is shown in red, the lowest-energy TA_1 branch in green, and the TA_2 branch in blue.

Although Eqns. 14 and 15 are not rigorous, they directly connect the phonon linewidth to the two-phonon density of states, and help explain the main physics. As shown in Fig. 2, up-conversion processes $D_\uparrow$ are prominent as $q \to 0$, but their contribution to the phonon linewidth is small. This is understood with Eqn. 14 in which the two-phonon densities of states are weighted by ω^2. Similarly, Eqn. 15 suggests that linewidths for most TA modes are zero as $T \to 0$ because down-conversion processes are prohibited.

Using experimental Grüneisen parameters of 2.0, 2.4 and 3.0[19], and average sound velocities of 3.687, 2.617 and 2.059 km/s for Cu, Ag and Au respectively, we calculated phonon linewidths at 600 K with Eqn. 14 and show the results in Fig. 4. The linewidths predicted with Eqn. 14 generally overestimate the phonon linewidths in comparison to those from the full calculations shown in Fig. 3. Nevertheless, the Grüneisen model for anharmonic force constants gives approximately the magnitude and shape of the phonon lineshape broadening. In further work, the individual mode Grüneisen parameters were obtained from the DFT calculations by examining the change in phonon frequencies with changes in the lattice parameter, and Eq. 11 was again used to obtain phonon coupling constants. The linewidths calculated with this more detailed model using mode Grüneisen parameters were in no better agreement with the full DFT calculations than the results shown in Fig. 4.

An interesting difference between the LA phonon linwidths of Cu, Ag and Au is the location of the most anharmonic mode (see Fig. 3), which corresponds to the highest peak in the two-phonon densities of states (Fig. 2). By analyzing the energies of the phonons in the final state of the decay process and comparing them with the one-phonon densities

of states, we find the final state energy spectra of these most anharmonic modes have the highest density of states for their decay. The central energy of the final state phonon spectra is at half of the energy of the initial phonon, and located where the one-phonon density of states is high. This can be generalized. The maximum linewidth of the LA modes is at least at twice the energy of the first Van Hove singularity in one-phonon density of states.

Finally, the full phonon linewidth comprises contributions from both phonon-phonon interactions and electron-phonon interactions. Because of the low electronic density of states near the Fermi level, the electron-phonon interactions in these noble metal systems are expected to be small[21]. The effects of electron-phonon coupling on phonon linewidths of Au were predicted by a previous first-principles study to be less than 0.01 meV[22], which is two orders of magnitude smaller than the effects of phonon-phonon coupling at room temperature. Interestingly, these calculations also gave prominent peaks in linewidth at the K and L points, much as seen in Fig. 3.

V. CONCLUSIONS

A systematic first-principles study of lattice anharmonicity and phonon linewidths was performed for the noble metals Cu, Ag and Au using density functional theory with phonon-phonon scattering theory. A direct supercell method was used to obtain both harmonic and third-order anharmonic force constants. While large supercells and fine k-grids are required for accurate forces due to the long-range interactions in these metal systems, the dominant contribution to the phonon linewidth is from the anharmonic force constants between nearest neighbors. The phonon linewidths of Cu, Ag and Au are comparable. The LA phonons of maximum linewidth are at different q-points for these three metal systems owing to differences in their final state spectra. For Cu, Ag, and Au, these peak LA linewidths occur at energies at least twice that of the first TA Van Hove singularity in the one-phonon densities of states. A simple Grüneisen model for the anharmonic phonon coupling constants can separate the third-order anharmonic potential from the scattering kinematics and connect directly the two-phonon densities of states with the phonon linewidth. Although not rigorous, this model predicts phonon linewidths that are in semiquantitative agreement with full calculations for Cu, Ag and Au. An energy factor before the two-phonon densities of states boosts the contribution from down-conversion processes, depresses the contribution from the up-conversion processes, and causes the maximum phonon linwidth to lie away from the center of the Brillouin zone. With its lower phonon energy and comparable phonon broadening as copper and silver, gold is the most anharmonic of these three noble metals.

VI. ACKNOWLEDGEMENT

This work was supported by the Department of Energy through the Basic Energy Sciences Grant DE-FG02-03ER46055, and benefitted from DANSE software developed under NSF Grant No. DMR-0520547.

[1] X. Tang, Chen W. Li and B. Fultz, Phys. Rev. B 82, 184301 (2010).
[2] P. E. Hopkins, et. al., J. Appl. Phys. 108, 104907 (2010).
[3] A. Larose and B. N. Brockhouse, Can. J. Phys. 54, 1990 (1976).
[4] M. Zoli, G. Santoro, V Bortolani, A. A. Maradudin and R. F. Wallis, Phys. Rev. B 41, 7507 (1990).
[5] A. A. Maradudin and A. E. Fein, Phys. Rev. 128, 2589 (1962).
[6] R. A. Cowley, Rep. Prog. Phys. 31, 123 (1968).
[7] C.Z. Wang, C. T. Chan and K. M. Ho, Phys. Rev. B 42, 11276 (1990).
[8] A. Debernardi, Phys. Rev. B 57, 12847 (1998).
[9] G. Deinzer, G. Birner and D. Strauch, Phys. Rev. B 67, 144304 (2003).
[10] G. Kresse and J. Furthümller, Comput. Mater. Sci. 6, 15 (1996).
[11] G. Kresse and J. Hafner, Phys. Rev. B 47, 558 (1993).
[12] G. Kresse and J. Furthmüller, Phys. Rev. B 54, 11169 (1996).
[13] P. E. Blöchl, Phys. Rev. B 50, 17953 (1994).
[14] G. Kresse and D. Joubert, Phys. Rev. B 59, 1758 (1999).
[15] B. Grabowski, T. Hickel and J. Neugebauer, Phys. Rev. B 76, 024309 (2007).
[16] P. H. Dederichs, H. Schober, D. J. Sellmyer, Metals: Phonon States, Electron States and Fermi Surfaces, edited by K.-H. Hellwege, J. L. Olsen. (Springer-Verlag, Berlin, 1981) Landolt-Bornstein, New Series, Group III, Vol. 13, Pt. a.
[17] M. Lax, P. Hu and V. Narayanamurti, Phys. Rev. B 23, 3095 (1981).
[18] P. G. Klemens, in Solid-State Physics, edited by F. Seitz and D. Turnbull (American Press, New York, 1958), Vol. 7, p. 1.
[19] Y. Hiki, J. F. Thomas Jr. and A. V. Granato, Phys. Rev. 153, 764 (1967).
[20] Kazuo Okubo and Shin-ichiro Tamura, Phys. Rev B 28, 4847 (1983).
[21] Z. Lin, L. V. Zhigilei and V. Celli, Phys. Rev. B 77, 075133 (2008)
[22] R. Bauer, A. Schmid, P. Pavone, and D. Strauch, Phys. Rev. B 57, 11276 (1998).